Chemical Engineering Journal 144 (2008) 420–430

Contents lists available at ScienceDirect

Chemical Engineering Journal

journal homepage: www.elsevier.com/locate/cej

Lead uptake by algae *Gelidium* and composite material particles in a packed bed column

Vítor J.P. Vilar, Cidália M.S. Botelho, Rui A.R. Boaventura*

LSRE-Laboratory of Separation and Reaction Engineering, Departamento de Engenharia Química, Faculdade de Engenharia da Universidade do Porto, Rua Dr. Roberto Frias, 4200-465 Porto, Portugal

ARTICLE INFO

Article history:
Received 14 December 2006
Received in revised form 6 February 2008
Accepted 20 February 2008

Keywords:
Biosorption
Lead(II)
Gelidium
Composite material
Packed bed column

ABSTRACT

Biosorption of lead ions was studied in a flow-through column packed with red algae *Gelidium* and a composite material (industrial algal waste from the agar extraction process immobilized with polyacrylonitrile). Experiments were performed in order to study the effect of important design parameters such as flow rate and influent pH. The breakthrough curves for lead and proton concentrations were obtained in saturation and elution studies. Macroscopically, when the flow rate increases, the residence time in the bed decreases, and the column saturation is faster achieved and the sharpness of the breakthrough curves increases. Microscopically, increasing the flow rate, the film diffusion resistance decreases. For higher values of the influent pH, the breakthrough time increases, due to the greater metal uptake capacity at the equilibrium. Considering the effectiveness of lead desorption from loaded biomass, we concluded that desorption was 100% effective and rapid, even for high values of the solid to liquid ratio, leading to high values of the concentration factor. The column packed with composite material was operated in two consecutive adsorption–desorption cycles, without any changes in the metal uptake capacity. A mathematical model based on external and intraparticle mass transfer was developed to simulate the breakthrough curves in the adsorption and desorption processes.

1. Introduction

In 1990, 5.627×10^6 tonnes of lead were consumed worldwide [1]. Mining, smelting and refining, as well as the manufacture of lead-containing compounds and goods, can give rise to lead emissions [2]. Traditional methods used to remove this toxic metallic ion from industrial wastewaters before discharge into natural water bodies, include coagulation and precipitation, ion-exchange, membrane separation and electrolytic technologies. Coagulation and precipitation processes lead to a high consumption of reagents and leave behind "hazardous sludge", which needs to be safely disposed off [3]. Ion-exchange (€20–40 kg^{-1}), activated carbon adsorption (€10–20 kg^{-1}) and membrane (€30–50 m^2) processes are expensive, particularly for large-scale clean-up operations, such as, for example, mining water treatment [3]. Those processes may also be ineffective for low metal concentrations (<100 $mg\,l^{-1}$) [3]. Alternative technologies are required to reduce toxic metal concentrations into environmental acceptable levels at affordable costs [3–5]. Biosorption, as it has been perceived so far, could be considered for its economic edge (€3–5 kg^{-1}) as a possible alternative technique for metal removal/recovery [3]. Biosorption is based on the passive sequestration by non-living biomass, containing many types of different chemically active groups that show some tendencies to uptake other chemical substances or ions, attracting them from solution and binding them to the biomass surfaces [3,6,7]. Biosorption of lead has been investigated using different kinds of marine algae, such as brown algae (*Sargassum hystrix*, *Sargassum natans*, *Padina pavonia*, *Fucus vesiculosus*, *Ascophyllum nodosum*), red algae (*Chondrus crispus*, *Galaxaura marginata*, *Palmaria palmate*, *Gracilaria corticata*, *Gracilaria canaliculata* and *Polysiphonia violacea*) and green algae (*Codium taylori*, *Ulva lactuca* and *Cladophora glomerata*) [8,9]. Other sorbents have been also applied, such as red mud-an aluminium industry waste [10], lignin obtained from black liquor-a paper industry waste material [11], waste brewery biomass [12], activated slag-a blast furnace waste [13] and others.

Biosorption of lead ions using red algae *Gelidium* and a composite material in a batch system was previously studied [14–16]. From these studies, it was concluded that biosorption of metal ions is due to negatively charged carboxylic groups present in the cell wall of the biosorbents at pH < 7. The mechanism of biosorption has been established as a combination of adsorption and ion-exchange between the metal cations present in solution and protons or other ions (Na^+, K^+) bound to carboxylic groups. For high proton

* Corresponding author. Tel.: +351 225081683; fax: +351 225081674.
E-mail addresses: vilar@fe.up.pt (V.J.P. Vilar), cbotelho@fe.up.pt (C.M.S. Botelho), bventura@fe.up.pt (R.A.R. Boaventura).

1385-8947/$ – see front matter © 2008 Elsevier B.V. All rights reserved.
doi:10.1016/j.cej.2008.02.020

Nomenclature

a_p	specific area for thin plates particles
C_b	metal concentration in the bulk (mg or mmol metal/l fluid)
C_{b_0}	initial metal concentration in the bulk (mg or mmol metal/l fluid)
C_E	feed concentration (mg or mmol metal/l fluid)
C_f	metal concentration in the film (mg or mmol metal/l fluid)
C_{final}	metal concentration in the solution at the end of the saturation or elution process (mg or mmol metal/l fluid)
C_H	equilibrium concentration of proton in the fluid phase (mmol proton/l fluid)
C_M	equilibrium concentration of metal in the fluid phase (mmol metal/l fluid)
C_T	total (lead + acid) liquid concentration (mmol/l fluid)
C_{T_0}	initial total (lead + acid) liquid concentration (mmol/l fluid)
C_{T_E}	total feed (acid) liquid concentration (mmol/l fluid)
d_p	particle diameter (cm)
D_{ax}	axial dispersion coefficient (cm^2/s)
D_h	homogeneous diffusion coefficient (cm^2/s)
D_m	molecular diffusivity of the metal ion in solution (cm^2/s)
k_f	film mass transfer coefficient (cm/s)
k_p	mass transfer coefficient for intraparticle diffusion (cm/s)
K_H	equilibrium proton constant (l fluid/mmol H)
K_M	equilibrium metal constant (l fluid/mmol M)
K_L	equilibrium constant of Langmuir (l fluid/mg M)
K_H^M	selectivity coefficient between ion M in the particle and H in solution
L	bed length (cm)
N_d	number of mass transfer units by intraparticle diffusion
N_f	number of mass transfer units by film diffusion
Pe	axial Peclet number based on the bed length
Pe_p	axial Peclet number based on the particle diameter (spherical) or width (thin plate)
pH_{SE}	pH of feed solution
pH_{CI}	initial pH of interstitial fluid inside the column
pH_{CF}	final pH of interstitial fluid inside the column
$\langle q \rangle$	average metal concentration in the solid phase (mg or mmol metal/g biomass)
q_E	solid phase concentration in equilibrium with C_E (mg or mmol metal/g biomass)
q_H	equilibrium concentration of proton in the biomass (mmol proton/g biomass)
q_M	equilibrium concentration of metal in the biomass (mg or mmol metal/g biomass)
q_{M_0}	metal concentration in the solid phase in equilibrium with C_{b_0} (mg or mmol metal/g biomass)
q^*	solid phase concentration in equilibrium with C_f (mg or mmol metal/g biomass)
Q_{max}	concentration of carboxylic groups or maximum capacity of biomass (mg or mmol/g biomass)
R	half of thickness of the thin plate (cm)
Sh	Sherwood number
t	time (s)
t_{Bp}	breakthrough time (s)
t_{st}	stoichiometric time (s)
T	temperature (°C)
u_i	interstitial fluid velocity (cm/s)
V_f	interstitial fluid volume (cm^3)
W	mass of biosorbent (g)
x	axial position normalized by the bed length
$\langle y \rangle$	dimensionless average concentration in the solid phase
y_b	dimensionless concentration in the fluid phase
y_f	dimensionless concentration in the fluid phase at the film
y_T	dimensionless total concentration in the fluid phase
y^*	dimensionless concentration in the solid phase at the particle surface
z	bed axial position (cm)

Greek letters

ε	porosity of the bed
τ	space time (s)
τ_d	time constant for intraparticle diffusion
τ_f	time constant for film diffusion
θ	dimensionless time
ρ_{ap}	apparent density of particles (g solid/cm^3 particle)
ξ	adsorber capacity factor for saturation
ξ'	adsorber capacity factor for desorption

concentration, the uptake capacity of metal ions decreases due to the competition with protons to the binding sites [14,15].

In this work, we investigated the performance of the same biosorbents to treat lead contaminated water in a packed bed column. The influence of the flow rate and pH of the feed stream on the breakthrough curve was analysed, as well as the possibility of regenerating the biosorbents. A mass transfer model was developed to describe the biosorption and desorption in the continuous packed bed column.

2. Materials and methods

2.1. Preparation of biosorbents

An algal waste from agar extraction industry was immobilized with an organic polymer (polyacrylonitrile-PAN) and used in this study as well as red algae *Gelidium*, which is the raw material for agar extraction. *Gelidium sesquipedale* is a red algae, harvested in the coasts of Algarve and São Martinho do Porto, Portugal. The industrial algal waste is composed essentially by 35% of algae *Gelidium* after agar extraction and 65% of diatomaceous earth used as filtration aid in the extraction process. To prepare the composite particles, fibrous PAN was first dissolved in dimethyl sulfoxide (DMSO) during 1–2 h. The powdered active component (industrial algal waste) was gradually added to PAN solution under stirring and the suspension mixed for about 30 min. Homogeneous suspension was then dispersed into water (coagulation bath) at room temperature. Beads formed in the water bath were washed with distilled water, separated by filtration on Buchner funnel and dried at about 30–40 °C. A more detailed description of the characteristics and preparation of both materials were presented in previous works [16,17].

2.2. Preparation of lead solution

Pb(II) solutions were prepared by dissolving a weighed quantity of anhydrous $PbCl_2$ (Merck-Schuchardt with purity >98%) in dis-

tilled water. The pH of each solution was adjusted to the required value with HNO_3 and NaOH solutions.

2.3. Column experiments

Experiments were performed in a glass jacketed column (Sigma C 5794) with an inner diameter, i.d. = 2.5 cm, and length, L = 15 cm, packed with algae *Gelidium* or composite material. The apparent density of the biosorbents determined by mercury intrusion (PORESIZER 9320) is 1.34 and 0.25 g cm^{-3}, respectively, for *Gelidium* and composite material [18]. A known quantity of *Gelidium* or composite material (≈10 g) was placed into the column. The lead solution (≈50 mg l^{-1}) was pumped downflow (peristaltic pump Gilson Minipuls 2) through the column at different flow rates (2, 4, 8 and 11 ml min^{-1}). Column effluent samples were collected at pre-defined times by a programmable fraction collector (Gilson FC 203B Fraction Collector) and analysed by atomic absorption spectrophotometry (GBC 932 Plus AAS). The pH of the effluent was also recorded. After column exhaustion, the loaded biomass with lead was regenerated with 0.1 M HNO_3, using a flow rate of 8 ml min^{-1}. The collection and analysis of the outlet samples were done as for the sorption protocol. After elution, the biomass bed was washed with distilled water until effluent pH stabilization near the inlet pH. The regenerated bed was reused in a next cycle. The column and all glassware were cleaned by washing with nitric acid (20%) and distilled water.

3. Theoretical approach

3.1. Equilibrium model

A mathematical equilibrium model has been developed assuming one kind of active sites (carboxylic groups) in the cell wall, which are responsible for metal biosorption at pH < 7.0, and for the competition between metal ions and protons [19]. The model is based on the apparent equilibrium binding constants, K_H and K_M for H^+ and M^{2+}, respectively. The total metal uptake can be calculated as:

$$q_M = \frac{Q_{max} K_M C_M}{1 + K_H C_H + K_M C_M} \quad (1)$$

This equation can be converted in the Langmuir equation:

$$q_M = \frac{Q_{max} K_L C_M}{1 + K_L C_M} \quad (2)$$

where

$$K_L = \frac{K_M}{1 + K_H C_H} \quad (3)$$

From the values of K_M, K_H it is possible to calculate the Langmuir equilibrium constant, K_L, for each pH.

3.2. Fixed bed operation

3.2.1. Saturation

A model was developed with the following assumptions: isothermal operation, axial dispersed plug flow of the fluid phase, adsorption equilibrium described by the Langmuir isotherm, external (film) resistance to mass transfer and internal mass transfer resistance described by the LDF approximation. The dimensionless equations of the mass transfer model, developed in a previous work [20], are:

Mass conservation in the fluid around particles:

$$\frac{\partial y_b(x,\theta)}{\partial \theta} = \frac{1}{Pe}\frac{\partial^2 y_b(x,\theta)}{\partial x^2} - \frac{\partial y_b(x,\theta)}{\partial x} - \xi N_d [y^*(x,\theta) - \langle y(x,\theta)\rangle] \quad (4)$$

Mass conservation inside particles (linear driving force, LDF):

$$\frac{d\langle y(x,\theta)\rangle}{d\theta} = N_d [y^*(x,\theta) - \langle y(x,\theta)\rangle] \quad (5)$$

If there is no accumulation in the fluid film surrounding the particles:

$$\frac{d\langle y(x,\theta)\rangle}{d\theta} = \frac{N_f}{\xi}[y_b(x,\theta) - y_f(x,\theta)] \quad (6)$$

Equalling Eqs. (5) and (6) we get:

$$[y^*(x,\theta) - \langle y(x,\theta)\rangle] = \frac{N_f}{\xi N_d}[y_b(x,\theta) - y_f(x,\theta)] \quad (7)$$

The dimensionless equilibrium is given by:

$$y^*(x,\theta) = \frac{(1 + K_L C_E) y_f(x,\theta)}{1 + K_L C_E y_f(x,\theta)} \quad (8)$$

with the initial and boundary conditions:

$$\theta = 0 y_b(x,0) = y_f(x,0) = \langle y(x,0)\rangle = 0 \quad (9)$$

$$x = 0 - \frac{1}{Pe}\frac{\partial y_b(x,\theta)}{\partial x} + y_b(x,\theta) = 1 \quad (10)$$

$$x = 1 \left.\frac{\partial y_b(x,\theta)}{\partial x}\right|_{x=1} = 0 \quad (11)$$

The dimensionless variables are defined as:

$$x = \frac{z}{L}, \quad \theta = \frac{t}{\tau}, \quad y_b(x,\theta) = \frac{C_b(z,t)}{C_E}, \quad y_f(x,\theta) = \frac{C_f(z,t)}{C_E},$$

$$\langle y(x,\theta)\rangle = \frac{\langle q(z,t)\rangle}{q_E}, \quad y^*(x,\theta) = \frac{q^*(z,t)}{q_E}, \quad \tau = \frac{L}{u_i}, \quad \tau_d = \frac{R^2}{D_h},$$

$$\tau_d^* = \frac{1}{k_p a_p} = \frac{\tau_d}{3}, \quad \tau_f = \frac{\varepsilon}{(1-\varepsilon)}\frac{1}{k_f a_p}, \quad (12)$$

and the dimensionless parameters as:

$$\xi = \frac{(1-\varepsilon)}{\varepsilon}\rho_{ap}\frac{q_E}{C_E}, \quad N_f = \frac{\tau}{\tau_f} = \frac{(1-\varepsilon)}{\varepsilon}k_f a_p \tau,$$

$$N_d = \frac{\tau}{\tau_d^*} = k_p a_p \tau, \quad Pe = \frac{u_i L}{D_{ax}} \quad (13)$$

where $q_E = Q_{max} K_L C_E / [1 + K_L C_E]$ is the solid phase concentration in equilibrium with C_E.

The partial differential Eqs. (4) and (5) in conjunction with the initial, Eq. (9), and boundary conditions, Eqs. (10) and (11), were solved by the PDECOL package [21], where $y_f(x,\theta)$ is obtained by solving Eq. (7) and the equilibrium is given by the Langmuir isotherm (Eq. (8)).

3.2.2. Elution

The desorption was considered as an ion exchange process, where the metal ions are released into the solution by exchange with the protons, in an approximately stoichiometric relation as in the exchange between copper ions and protons [22]. Since the proton has a higher affinity to the carboxylic groups than copper and lead ions, which have similar affinities, the exchange rate can be considered equal for both metals. Equilibrium desorption was well described by the mass action law [22]:

$$y^* = \frac{K_H^M y_b}{y_T + (K_H^M - 1) y_b} \quad (14)$$

where K_H^M and Q_{max} values are 0.93 and 1.1, 0.36 and 0.16 mmol g^{-1}, respectively for *Gelidium* and composite material [22].

An elution model based on the same assumptions as the saturation model, with exception of equilibrium, which is now described by the mass action law, was developed. So, Eqs. (4), (5) and (7)

are still valid if the concentrations in the liquid and solid phase are expressed in mmol instead of mg. As we have two components, it is necessary to take into account the conservation of the total concentration in the fluid phase, considering that after biomass saturation, the amount of metal ions and protons bound to the solid phase is equal to the maximum concentration of active sites [23,24]. So, the partial derivative in time is zero ($\partial(\langle C_H\rangle + \langle C_H\rangle)/\partial t = \partial Q_{max}/\partial t = 0$).

Then,

$$\frac{\partial y_T(x,\theta)}{\partial \theta} = \frac{1}{Pe}\frac{\partial^2 y_T(x,\theta)}{\partial x^2} - \frac{\partial y_T(x,\theta)}{\partial x} \quad (15)$$

The dimensionless variables are:

$$x = \frac{z}{L}, \quad \theta = \frac{t}{\tau}, \quad y_b(x,\theta) = \frac{C_b(z,t)}{C_{T_0}}, \quad y_f(x,\theta) = \frac{C_f(z,t)}{C_{T_0}},$$

$$y_T(x,\theta) = \frac{C_T(z,t)}{C_{T_0}}, \quad \langle y(x,\theta)\rangle = \frac{\langle q(z,t)\rangle}{Q_{max}}, \quad y^*(x,\theta) = \frac{q^*(z,t)}{Q_{max}} \quad (16)$$

The dimensionless parameters are the same considered before, except for the column capacity factor, which is now defined as:

$$\xi' = \frac{(1-\varepsilon)}{\varepsilon}\rho_{ap}\frac{Q_{max}}{C_{T_0}} \quad (17)$$

The initial and boundary conditions are:

$$\theta = 0, \quad y_b(x,0) = \frac{C_{b_0}}{C_{T_0}}, \quad y_f(x,0) = \frac{C_{b_0}}{C_{T_0}},$$

$$y_T = 1, \ \langle y(x,0)\rangle = \frac{q_{M_0}}{Q_{max}} \quad (18)$$

$$x = 0, \quad -\frac{1}{Pe}\frac{\partial y_b(x,\theta)}{\partial x} + y_b(x,\theta) = 0 \quad (19)$$

$$-\frac{1}{Pe}\frac{\partial y_T(x,\theta)}{\partial x} + y_T(x,\theta) = \frac{C_{T_E}}{C_{T_0}} \quad (20)$$

$$x = 1, \quad \left.\frac{\partial y_b(x,\theta)}{\partial x}\right|_{x=1} = \left.\frac{\partial y_T(x,\theta)}{\partial x}\right|_{x=1} = 0 \quad (21)$$

where C_{T_E} is the molar concentration of the feed solution (0.1 M HNO_3) and C_{T_0} is the sum of the metal and proton concentration in the interstitial fluid inside the column at the end of the saturation process.

The partial differential Eqs. (4), (5) and (15) in conjunction with the initial, Eq. (18), and boundary conditions, Eqs. (19)–(21), were solved by the PDECOL package [21], where $y_f(x,\theta)$ is obtained by solving Eq. (7) and the equilibrium is given by the mass action law (Eq. (14)).

4. Results and discussion

The model parameters of Eq. (1) were obtained as [15]: $Q_{max} = 0.26 \pm 0.01$ and 0.096 ± 0.003, $pK_H = \log K_H = 3.92 \pm 0.07$ and 4.7 ± 0.1 and $pK_M = \log K_M = 4.02 \pm 0.06$ and 4.6 ± 0.1, respectively, for *Gelidium* and composite material.

4.1. Effect of flow rate

The effect of flow rate on the biosorption of lead ions was studied by changing the flow rates from 2 to 8 ml min^{-1} and 4 to 11 ml min^{-1}, respectively, for the composite material and algae *Gelidium*. The breakthrough curves and the pH profiles are illustrated in Fig. 1(a) and (b). Increasing the flow rate, the breakthrough time (t_{Bp}) and the final or saturation time (t_f) decreases, as a higher amount of lead ions is fed to the column in a shorter time interval. Macroscopically, increasing the flow rate corresponds to increase

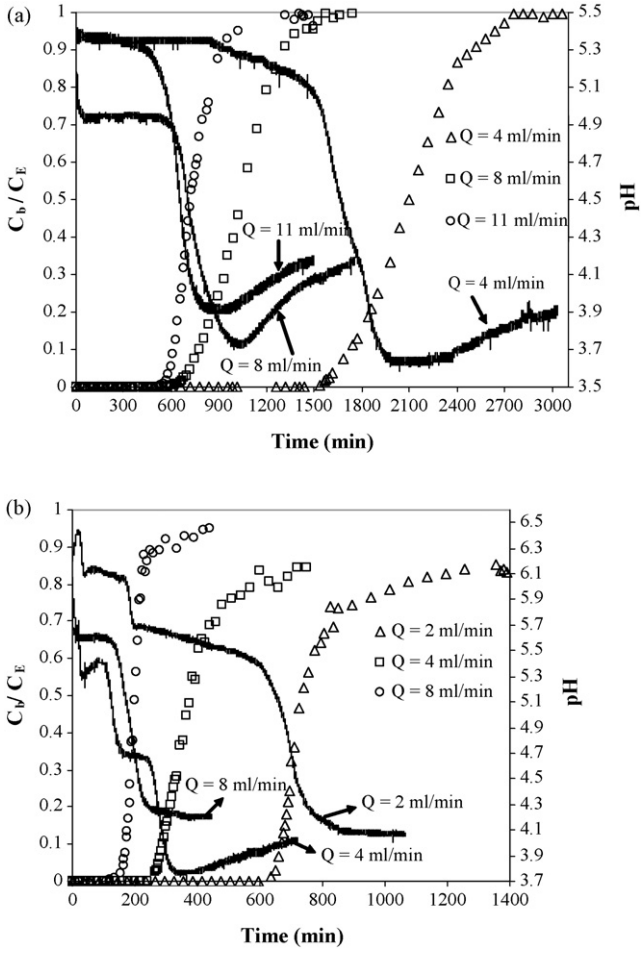

Fig. 1. Influence of flow rate on the breakthrough curve for lead biosorption and pH profile: (a) red algae *Gelidium* and (b) composite material.

the superficial velocity inside the column and the breakthrough curve becomes sharper. Representing the breakthrough curves as a function of the dimensionless time, it can be seen (Fig. 2(a) and (b)) that the three curves merge on a single curve, in the case of the algae *Gelidium* (Fig. 2(a)), suggesting that the influence of the flow rate on the biosorption only affects the equilibrium time. So, for higher flow rates the residence time decreases and the time necessary to reach the saturation of the material diminishes. The lead uptake by the algae is independent on the flow rate in the study range, approximately 37.4 mg Pb(II) g^{-1}. However, in the biosorption of lead by the composite material, the breakthrough curves for different flow rates do not merge into a single curve. The dimensionless time of breakthrough varies with the flow rates in the following order $4 < 2 < 8$ ml min^{-1}, corresponding to lead uptakes of 6.2, 7.0 and 7.3 mg g^{-1}. These differences may be due to the different pH profiles observed (Fig. 2(b)) and the equilibrium pH achieved (4.0, 4.1 and 4.2, respectively, for the flow rates 4, 2 and 8 ml min^{-1}).

A mass transfer model considering mass transfer resistances in the film and in the particle, where the equilibrium relationship is given by the Langmuir equation (Eq. (2)) was applied to the experimental results. The Langmuir equilibrium constants were determined by the discrete model (K_H and K_M) (Eq. (1)), considering the equilibrium pH inside the column to calculate the Langmuir affinity constant by Eq. (3). The equilibrium pH inside the column was considered as the final pH value of the experiment, obtained by the pH profiles illustrated in Fig. 1(a) and (b), respectively for *Gelidium* and composite material.

Table 1
Operation parameters for the breakthrough and elution curves

No.	Type	Q (ml/min)	pH_{SE}	pH_{CI}	pH_{CF}	C_E/C_{b_0} (mg l^{-1})	C_{final} (mg l^{-1})	T (°C)	W (g)	ε	τ (min)
Algae *Gelidium*											
1	S	4.0	5.3	5.4	3.9	47.3/0	47	20	10.6	0.893	16.4
2	E	7.9	1.0	4.0	1.0	0/47.0	0.47	20	10.6	0.893	8.3
3	S	8.0	5.3	5.1	4.2	47.3/0	47.0	20	10.6	0.893	8.3
4	E	8.0	1.0	4.2	1.0	0/41.4	0.15	20	10.6	0.893	8.3
5	S	11.0	5.4	5.4	4.2	48.5/0	46.8	20	10.7	0.892	6.0
6	E	11.0	1.0	4.2	1.0	0/46.8	0.05	20	10.7	0.892	6.0
7	S	8.0	4.0	4.1	3.6	49.6/0	43.5	20	11.1	0.888	8.2
8	E	8.0	0.94	3.6	0.94	0/43.5	0.01	20	11.1	0.888	8.2
9	S	8.0	3.0	3.0	3.0	52.2/0	52.2	20	10.4	0.895	8.2
10	E	8.0	0.95	2.8	0.95	0/52.2	0.17	20	10.4	0.895	8.2
Composite material											
11	S	2.0	5.2	6.1	4.0	47.6/0	40.0	20	8.9	0.513	18.9
12	E	8.0	0.85	4.0	0.85	0/40.0	0.1	20	8.9	0.513	4.7
13	S[a]	3.9	5.2	5.4	4.0	44.6/0	37.8	20	9.2	0.498	9.4
14	E[a]	8.5	1.0	4.1	1.0	0/20.4	0.5	20	9.2	0.498	4.3
15	S[b]	4.0	5.2	4.9	4.0	44.9/0	39.0	20	9.2	0.498	9.2
16	E[b]	8.0	1.0	4.0	1.0	0/39.0	0.6	20	9.2	0.498	4.6
17	S[a]	8.0	5.3	5.6	4.2	48.9/0	46.5	20	10.6	0.422	3.9
18	E[a]	8.0	1.0	4.2	1.0	0/46.5	0.5	20	10.6	0.422	3.9
19	S[b]	8.0	5.2	4.4	4.0	43.6	36.0	20	10.6	0.422	3.9
20	S	8.0	4.0	4.1	3.8	49.3/0	44.0	20	9.3	0.495	4.6
21	E	8.0	0.94	3.8	0.94	0/44.0	0.02	20	9.3	0.495	4.6
22	S	8.0	3.0	3.0	3.0	48.1/0	47.0	20	8.1	0.558	5.1
23	E	8.0	1.0	3.0	1.0	0/47.0	0.46	20	8.1	0.558	5.1

S, Saturation and E, elution.
[a] First cycle.
[b] Second cycle.

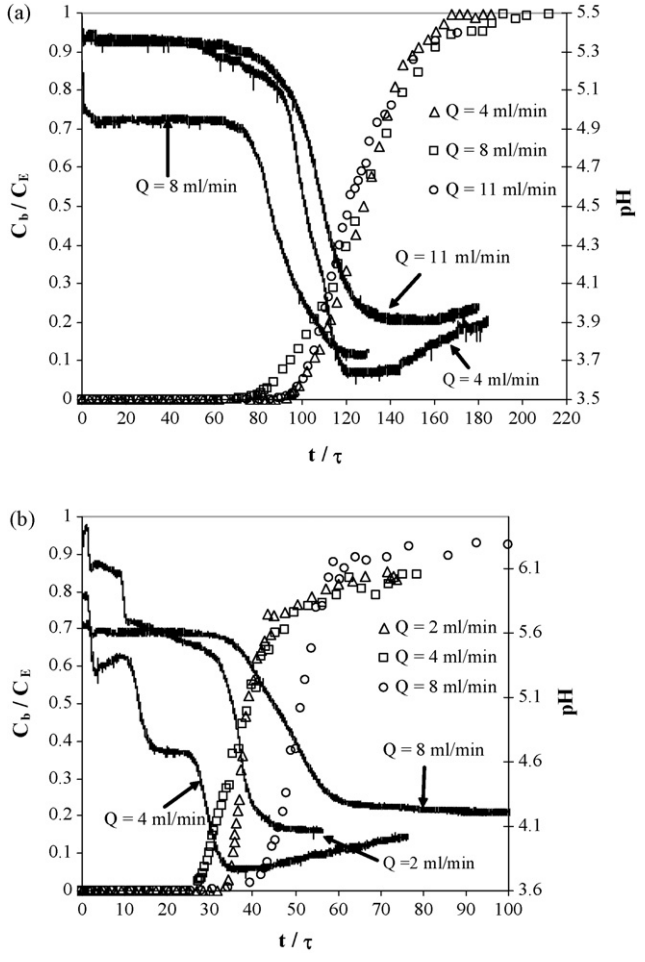

Fig. 2. Breakthrough curves for lead biosorption at three different flow rates and pH profiles as a function of the dimensionless time: (a) red algae *Gelidium* and (b) composite material.

The operation parameters are shown in Table 1. The homogeneous diffusion coefficient average value, ($D_h = 3.7 \times 10^{-8}$ and 2.5×10^{-8} cm^2 s^{-1}, respectively for *Gelidium* and composite material), was determined by batch dynamic studies at different pH values (5.3, 4 and 3) [15]. Assuming $Pe_p = u_i d_p / D_{ax} = 2$ [25]; $Pe = 2L/d_p$ is equal to 3000 and 332, respectively for the algae *Gelidium* and the composite material. $Pe_p = 2$ is valid for spherical particles ($d_p = 0.9$ mm for the composite material particles). For the algae *Gelidium* particles, that are like thin plates, we assumed $d_p = 2R$, where $2R$ is the width of the thin plate.

Fig. 3(a) and (b) illustrate the breakthrough curves simulated for *Gelidium*, and composite material, respectively, for different flow rates and $C_E \approx 50$ mg l^{-1}. The equilibrium parameters were chosen inside the interval of the standard deviation. In the adsorption of lead by algae *Gelidium*, the deviations relatively to the experimental results are higher for the lowest flow rate, and in the final and initial parts of the curve, probably due to the heterogeneity of the binding sites.

In the case of the composite material, the saturation of the biomass ($C_b/C_E = 1$) is achieved more slowly than the predicted by the mass transfer model (Fig. 3(b)) and the difference increases when decreasing the flow rate. The results suggest a slow diffusion of the metal ions to the binding sites, which is supported by the fact that the active component is involved by the polymer, and the metal ion has to diffuse through the pores between the algal particles inside the granules. This effect will be more accentuated if some organic compounds in solution complex the metal ion, increasing the radius of the species. On the other hand, once the biosorbent is heterogeneous, in the final part of the process only the binding sites with lower affinity by the metal ion are available, which contributes to lengthen the final part of the curve. The dotted lines in Fig. 3(b), obtained from the mass transfer model, using the equilibrium parameters determined in the batch system, predict a breakthrough time higher than that experimentally obtained. Decreasing the maximum uptake capacity, Q_{max}, by 50%, the model describes well the initial part of the experimental curve, but the

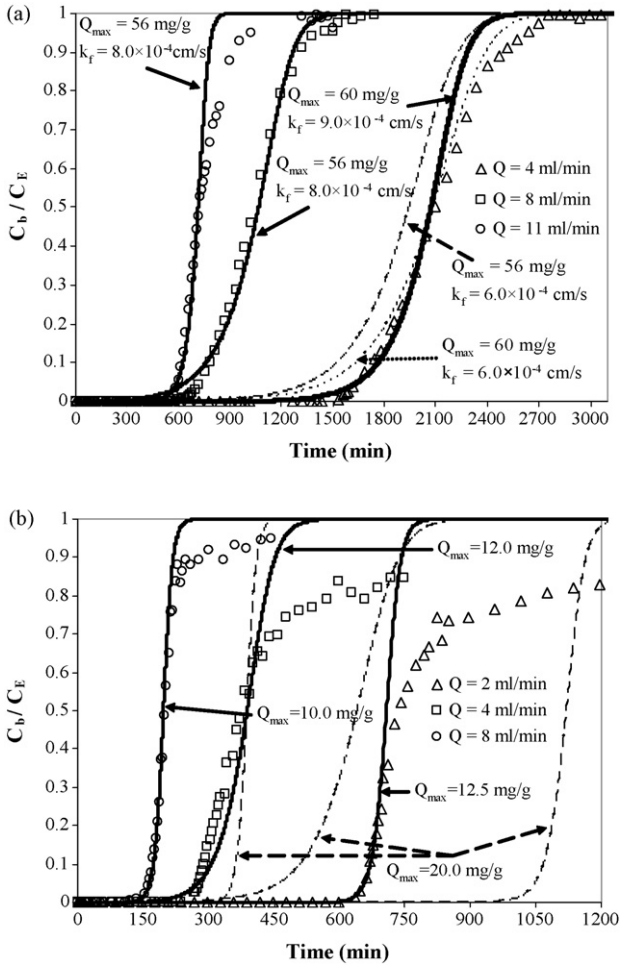

Fig. 3. Comparison of the experimental lead breakthrough curve and the calculated by the mass transfer model: (a) red algae *Gelidium* and (b) composite material. Influence of flow rate.

saturation is achieved earlier. This result suggests that only 50% of the binding sites are occupied by the metal with the affinity considered, and the remaining binding sites, with lower affinity, are occupied more slowly.

The change in the flow rate is expected to affect the film diffusion, but not the intraparticle diffusion. The higher the flow rate, the smaller the film resistance and the larger k_f. Due to the proximity of the values of flow rate, this trend was only verified for the two higher values of flow rate (Table 2). The film mass transfer coefficient was estimated by the number of Sherwood, $Sh = k_f d_p / D_m$, where D_m is the molecular diffusivity, which was calculated by the Nernst-Haskell equation [26], resulting $D_m = 9.3 \times 10^{-6}$ cm^2 s^{-1}. For an isolated spherical particle surrounded by a stagnant fluid, the limited value of Sherwood for low Reynolds number is 2.0, leading to $k_f = 3.7 \times 10^{-3}$ and 2.1×10^{-4} cm s^{-1}, respectively for the algae *Gelidium* and the composite material. The value obtained for the algae *Gelidium* has no significant meaning since the particles are like thin plate, and $Sh = 2$ is valid only for spherical particles. For the composite material, the values of k_f that better simulate the experimental results are higher than the obtained in the absence of agitation ($Sh = 2$), which proves that the mass transfer film decreased.

As $\xi N_d > N_f$, it is possible to conclude that the process is external mass transfer controlled. For $Q = 8$ ml min^{-1}, the film resistance is similar to the intraparticle resistance, for the composite material.

Generally, increasing the flow rate, the length of the mass transfer zone (MTZ) and the fraction of unused bed (LUB) increase, as shown in Table 2.

The optimization of the flow rate is essential for the implementation of a similar process at full scale. If the flow rate is too high, the saturation of the biosorbent is not achieved, and, consequently, the fraction of used bed is too low, ending the saturation cycle prematurely. When the flow rate is too low, the productivity is low, since the volume of the influent treated per unit of time is small. So, it is necessary to find out the optimal flow rate that maximizes the productivity and efficiency.

If the biosorption process is to be used as an alternative in wastewater treatment, the regeneration of the biosorbent may be crucially important to keep the processing costs low and open the possibility of recovering the metal(s) extracted from the liquid phase [3]. So, the regeneration of the biosorbents saturated with lead was studied using HNO_3 0.1 M as eluant. Observing Fig. 4(a) and (b) and calculating the amount of lead eluted, we concluded that desorption was complete. Desorption is also very rapid, occurring in the first 25 and 17.5 min, respectively, for *Gelidium* and composite material, considering a flow rate of 8 ml min^{-1}. Desorption at a flow rate of 11 ml min^{-1}, results in a faster release of the lead ions loaded (occurring in the first 20 min), explained by the lower residence time of the eluant. As the eluant is a strong acid the concentration front of the eluant drag off the lead ions easily to the end of the column. The utilization of a more concentrated eluant, allows to obtain high metal concentrations in the effluent (Table 3). These results indicate that for high S/L, desorption is 100% efficient and lead is recovered in small volumes, approximately 140 and 200 ml of HNO_3 0.1 M, respectively, for the composite material and algae *Gelidium*.

Table 2
Mass transfer parameters for biosorption of lead (effect of flow rate)

Q (ml min^{-1})	K_M (l mg^{-1})	Q_{max} (mg g^{-1})	ξ_p	ε	k_f (cm s^{-1})	N_d	$\xi_p N_d$	N_f	t_{st} (min)	t_{Bp} (min)	MTZ (cm)	LUB (%)
		56.0	115.0	0.893	6.0×10^{-4}	4.38	503.7	14.2				
4[a]	3.2×10^{-2}	60.0	123.2		9.0×10^{-4}	4.38	539.6	21.3	2066	1550	7.5	25.0
		60.0	123.2		6.0×10^{-4}	4.38	539.6	14.2				
8[a]	4.2×10^{-2}	56.0	124.9	0.893	8.0×10^{-4}	2.19	273.5	9.5	1038	644	11.4	38.0
11[a]	3.4×10^{-2}	56.0	117.1	0.892	3.0×10^{-3}	1.59	186.2	26.1	714	564	6.3	21.0
		20.0	59.6	0.515	5.0×10^{-4}	3.41	203.2	107.2				
2[b]	3.0×10^{-2}	12.5	36.3				123.8		715	635	3.3	11.1
		20.0	66.1	0.498	1.5×10^{-4}	1.69	111.7	17.1				
4[b]	3.0×10^{-2}	12.0	39.7				67.1		371	260	9.0	30.0
		20.0	99.1	0.422	5.0×10^{-4}	0.70	69.4	31.9				
8[b]	5.0×10^{-2}	10.0	49.5	0.422			34.7		205	134	10.4	34.8

[a] *Gelidium*: $Q_{max} = 54 \pm 2$ mg g^{-1}, $K_{Pb} = 0.025 \pm 0.007$ l mg^{-1} (pH_{CE} 3.9), $K_{Pb} = 0.033 \pm 0.008$ l mg^{-1} (pH_{CE} 4.2).
[b] Composite material: $Q_{max} = 20 \pm 1$ mg g^{-1}, $K_{Pb} = 0.03 \pm 0.01$ l mg^{-1} (pH_{CE} 4.0), $K_{Pb} = 0.05 \pm 0.01$ l mg^{-1} (pH_{CE} 4.2).

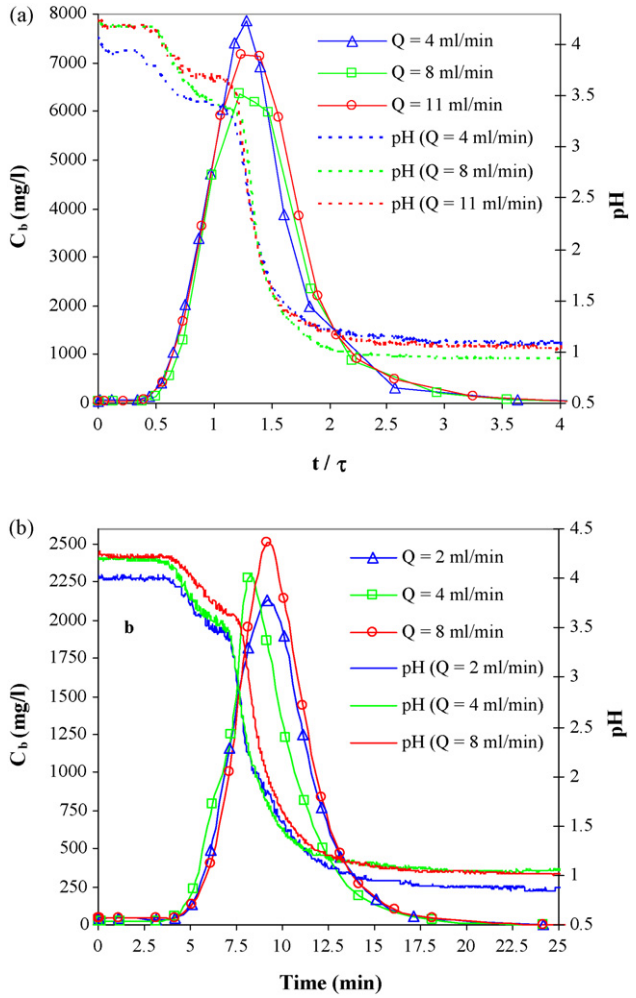

Fig. 4. Elution of lead by 0.1 M HNO_3 from biosorption column and pH profile: (a) red algae *Gelidium* and (b) composite material. The flow rates correspond to the saturation process.

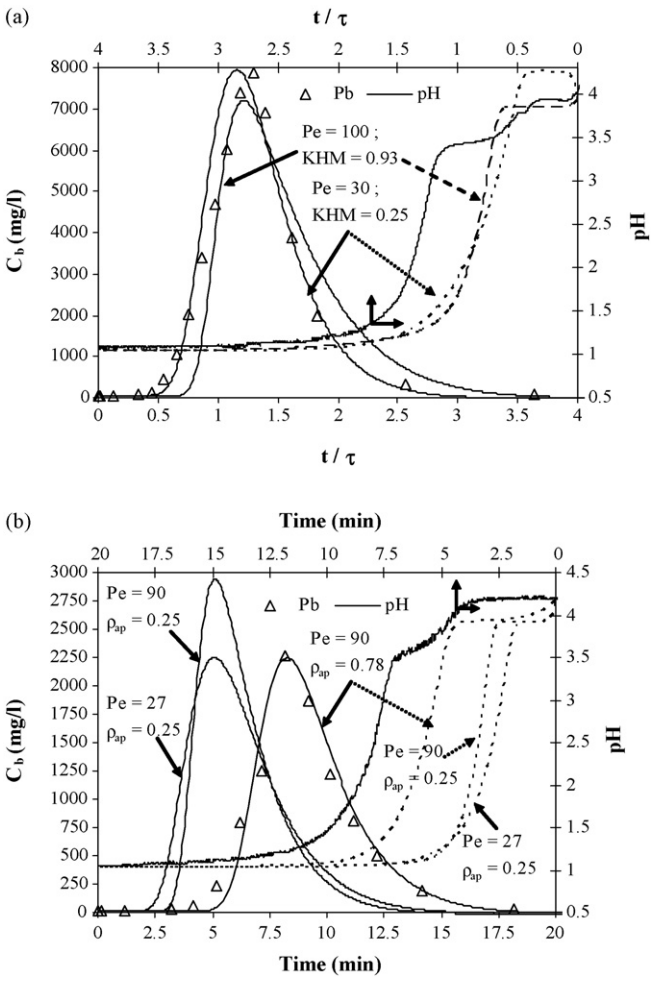

Fig. 5. Comparison of the experimental lead elution curve and the calculated by the mass transfer model: (a) red algae *Gelidium* and (b) composite material. Influence of flow rate.

When desorption process is 100% efficient, the concentration ratio, CR can be estimated as [22]:

$$\mathrm{CR} = \left(\frac{S}{L}\right) \frac{Q_{\max} K_{\mathrm{L}}}{1 + K_{\mathrm{L}} C_{\mathrm{final}}\,(\mathrm{adsorption})} \qquad (22)$$

Values of CR calculated by Eq. (22) are presented in Table 3. For algae *Gelidium*, the calculated values are lower than the experimental ones, as equilibrium is underestimated.

Table 3
Comparison between the solid to liquid ratio, *S*/*L*, the concentration ratio, CR, and the maximum concentration value at the end of the column, C_S (desorption of lead by red algae *Gelidium* and composite material)

Biosorbent	Q^a (ml min^{-1})	*S*/*L* (g l^{-1})	CR		C_S (mg l^{-1})
			Exp.	Calc.	
Gelidium	4	161	166	102	7868
	8	161	135	112	6369
	12	163	148	113	7160
Composite material	2	236[b]	53	52	2508
	4	251[b]	51	54	2272
	8	341[b]	44	58	2129

[a] Flow rate used in the adsorption process.
[b] $\rho_{ap} = 0.25$ g cm^{-3}.

The curves simulated by the mass transfer model, assuming film and particle resistances, and equilibrium given by the mass action law, are presented in Fig. 5(a) and (b). The value of the homogeneous diffusivity coefficient for lead ions was assumed to be equal to that obtained for copper ions ($D_h = 1.0 \times 10^{-7}$ and 3.0×10^{-7} cm^2 s^{-1}, respectively for *Gelidium* and composite material) [22]. The coefficient of selectivity (K_H^{Pb}) was also considered to be the same as determined in batch system for copper ions. The two adjustable parameters are the mass transfer film coefficient and the Peclet number. As the elution curves are very similar for all flow rates, we only present here the simulation of experiments 2 and 14. The simulated elution curves for the composite material, considering the apparent density of 0.25 g cm^{-3} are displaced to the left, compared with the experimental elution curve (Fig. 5(b)), suggesting that the calculated residence time (τ) is lower than the experimental one. Increasing the apparent density to 0.78 g cm^{-3}, bed porosity and residence time also increase, shifting to right the simulated elution curve. The apparent density value of 0.78 g cm^{-3} was obtained by considering the absence of pores larger than 60 Å diameter [18].

The feed of a strong eluant, such as 0.1 M HNO_3, leads to a faster diffusion. The same trend was obtained in the desorption of copper ions in a column system [20].

As observed in the saturation process, the particle mass transfer resistance is lower than the resistance in the film ($\xi N_d \gg N_f$, see Table 4), which means that the intraparticle lead ions diffusion is extremely rapid, as the result of the exchange with high diffusiv-

Table 4
Mass transfer parameters for elution of lead (effect of flow rate)

Biosorbent	K_H^M	Q_{max} (mmol g^{-1})	ξ'_p	ε	P_e	k_f (cm s^{-1})	N_d	$\xi'_p N_d$	N_f
Gelidium	0.93 0.25	0.36	180.7	0.893	100 30	3.0×10^{-3}	5.0	898.6	35.9
Composite material	1.1	0.16	150.0	0.840	90	4.0×10^{-4}	11.0	1650.0	6.7

ity protons. We can conclude that the elution process is apparently controlled by lead ions diffusion in the film. The curve of effluent pH simulated by the mass transfer model is also presented in Fig. 5(a) and (b). The simulated profiles of pH are not a perfect representation of the experimental trend, but show that elution is an ion exchange process.

4.2. Effect of Initial pH

The solution pH plays an important role in metal ion adsorption, as it was already concluded in equilibrium and kinetic experiments in batch system [14,15,27]. In order to examine the pH variation and effect on metal ion adsorption in fixed bed columns, the breakthrough curves for three different initial pH were analysed for algae *Gelidium* (pH: 5.0, 4.0 and 3.0) and composite material (pH: 5.6, 4.0 and 3.0), as illustrated in Fig. 6(a) and (b). The pH inside the column was initially adjusted to the value of the inlet stream.

From the breakthrough curves, it is possible to determine the quantity of protons released to solution and lead ions bound to the biosorbent. The ion exchange rate is approximately stoichiometric as determined in equilibrium experiments [15]. For initial pH 3, the effluent pH maintains almost constant during the experiment, as the uptake capacity is small due the competition with the high concentration of protons. For algae *Gelidium*, it can be observed that pH of the effluent after the breakthrough time increases. This occurs due to the fact that the algae active sites are almost saturated, and the release of protons to solution is small. Moreover, protons are easily neutralized by the continuous inlet lead solution at higher pH. In the case of the composite material, the final part of the pH profile slightly increases, because the saturation of the binding sites was not achieved yet, and the protons released to solution turn the effluent pH almost constant.

For higher values of the initial pH, the breakthrough time increases, since metal uptake capacity increases with pH, as observed in Fig. 6(a) and (b). This trend is due to the competition between the protons and metal ions to the binding sites. Carboxylic groups are protonated at low pH and metal binding is negligible. As pH increases, those groups dissociate, becoming negatively charged and then available to bind positively charged species in solution. Breakthrough curves for the initial pH 5.0 and 4.0 are very similar as observed in Fig. 6(a), with a small difference in the breakthrough time (7%), as the final pH values inside the column are similar. For pH 3, the breakthrough time decreases ≈56%, relatively to the experiment at initial pH 5.0. Observing Fig. 6(b), the final pH values

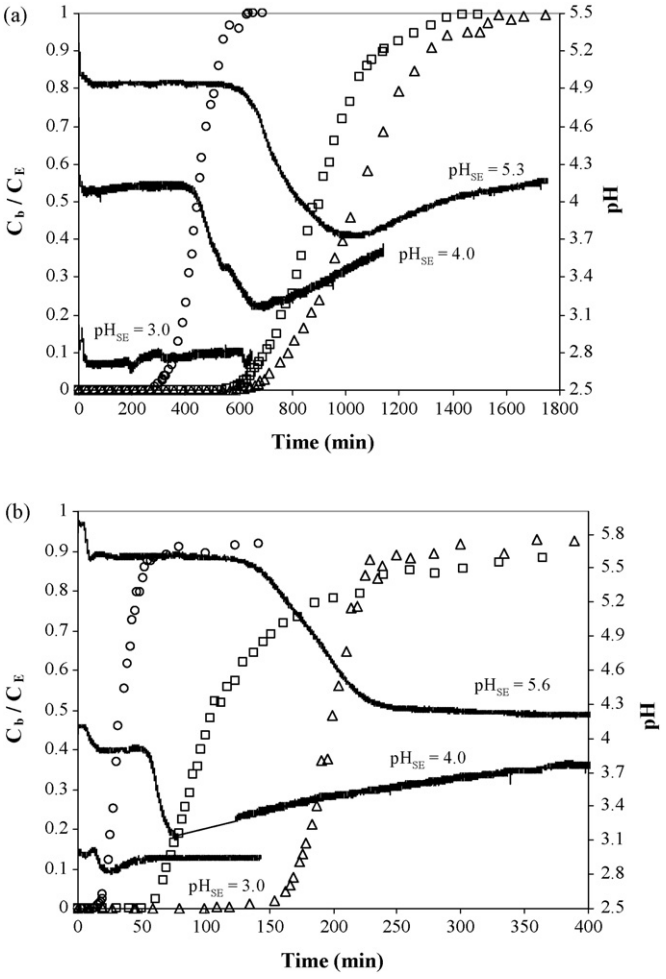

Fig. 6. Influence of initial pH on the breakthrough curve for lead biosorption and pH profile: (a) red algae *Gelidium* and (b) composite material. (△) pH_{SE} 5.3, (□) pH_{SE} 4.0, (○) pH_{SE} 3.0.

for the experiments 17, 20 and 22 are, respectively, 4.2, 3.8 and 3.0. The adsorption equilibrium given by the Langmuir isotherm is different for each case, giving different uptake capacities for the composite material. The breakthrough times in the experiments 20 and 22 are 82% and 87% lower than that obtained in the Experiment 17.

Table 5
Mass transfer parameters for biosorption of lead (effect of pH)

pH_{SE}	K_M (l mg^{-1})	Q_{max} (mg g^{-1})	ξ_p	ε	k_f (cm s^{-1})	N_d	$\xi_p N_d$	N_f	t_{st} (min)	t_{Bp} (min)	MTZ (cm)	LUB (%)
4.0[a]	2.5×10^{-2}	56.0	106.1	0.888	1.5×10^{-3}	2.18	231.3	18.6	888	598	9.8	32.9
3.0[a]	1.6×10^{-2}	39.0	53.7	0.895	2.2×10^{-3}	2.19	117.6	25.6	448	284	11.0	36.6
4.0[b]	2.1×10^{-2}	20.0 8.0	52.9 21.2	0.495	4.0×10^{-4}	0.82	43.4 17.4	22.4	105.5	47	16.6	55.5
3.0[b]	3.0×10^{-3} 3.0×10^{-3}	19.0	9.3	0.558	6.0×10^{-3}	3.3 0.93	30.9 8.6	292.8	52.8	35	10.1	33.7

[a] *Gelidium*: $Q_{max} = 54 \pm 2$ mg g^{-1}, $K_{Pb} = 0.020 \pm 0.005$ l mg^{-1} (pH_{CE} 4.0), $Q^*_{max} = 37.8$ mg g^{-1}, $K^*_{Pb} = 0.014 \pm 0.002$ l mg^{-1} (pH_{CE} 3.0) (asterisk appearing in values represents data obtained by the Langmuir equation at pH 3.0.).

[b] Composite material: $Q_{max} = 20 \pm 1$ mg g^{-1}, $K_{Pb} = 0.021 \pm 0.007$ l mg^{-1} (pH_{CE} 3.8); K_{Pb} 0.004 ± 0.001 l mg^{-1} (pH_{CE} 3.0).

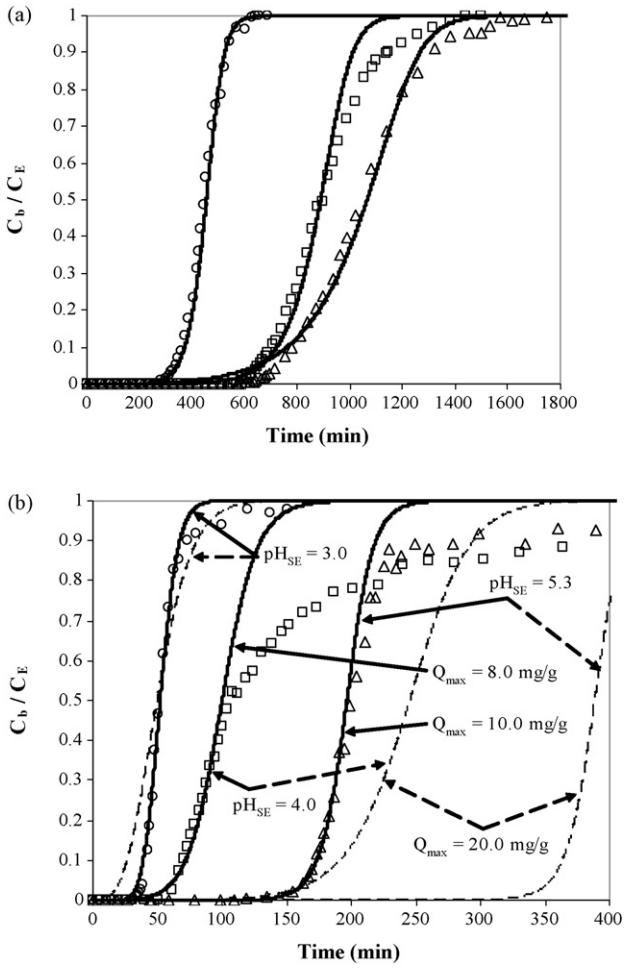

Fig. 7. Comparison of experimental lead breakthrough curve and the calculated by the mass transfer model: (a) red algae *Gelidium* and (b) composite material. Influence of initial pH. (△) pH_{SE} 5.3, (□) pH_{SE} 4.0, (○) pH_{SE} 3.0, (—) model.

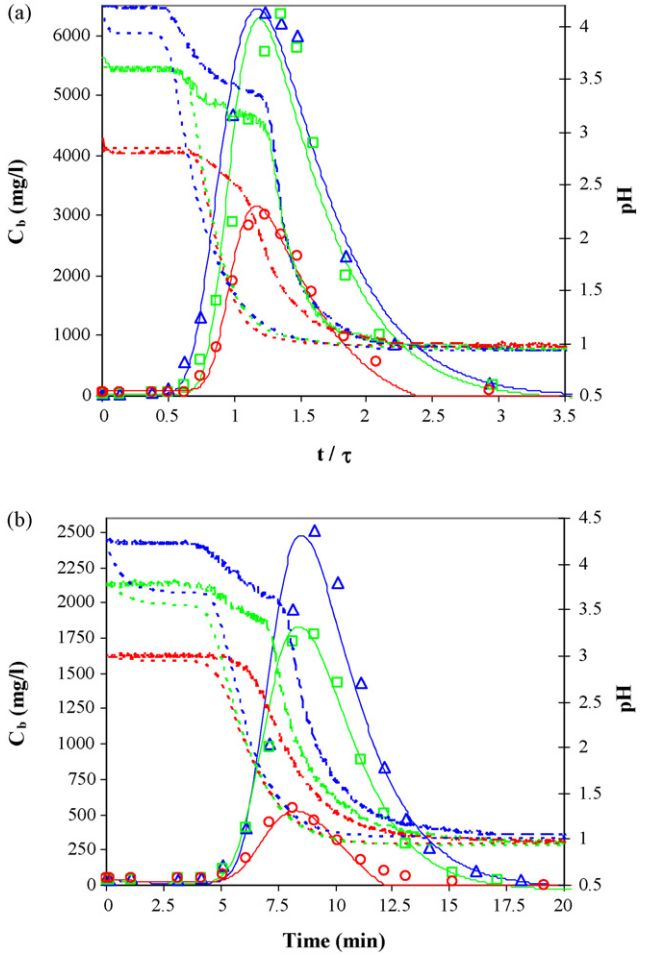

Fig. 8. Comparison of experimental lead elution curve and the calculated by the mass transfer model: (a) red algae *Gelidium* and (b) composite material. Influence of initial pH. Pb: (△) pH_{SE} 5.3, (□) pH_{SE} 4.0, (○) pH_{SE} 3.0, (——) Model pH_{SE} 5.3, (——) Model pH_{SE} 4.0, (——) Model pH_{SE} 3.0. pH: (——) pH_{SE} 5.3, (——) pH_{SE} 4.0, (——) pH_{SE} 3.0, (——) Model pH_{SE} 5.3, (——) Model pH_{SE} 4.0, (——) Model pH_{SE} 3.0.

Fig. 7(a) and (b) present the curves simulated by the mass transfer model for different initial pH values. The experimental results for the algae *Gelidium* are reasonably predicted by the mass transfer model (Table 5).

For the composite material, the final part of the breakthrough curves is elongated, due to the adsorption of the lead ions in low affinity sites, as mentioned above, and the simulated curves do not fit that part of the breakthrough curve. However, for pH 3 the simulated curve describes well the experimental breakthrough results using a value for the homogeneous diffusivity higher than that obtained in the batch system. This occurs because the binding sites with low affinity by the metal ions are probably protonated.

The dotted lines correspond to the mass transfer model, using the equilibrium parameters determined in the batch system. Decreasing the maximum uptake capacity, Q_{max}, by 50%, the model describes well the initial part of the experimental curve, but the saturation is achieved earlier, as it was previously concluded.

Desorption experiments were performed after saturation of the column. The experimental results and the respective simulated curves are presented in Fig. 8(a) and (b). Desorption is 100% efficient as the metal desorbed is in agreement with the amount

Table 6
Comparison between the solid to liquid ratio, *S*/*L*, the concentration ratio, CR, and the maximum concentration value at the end of the column, C_S (desorption of lead by red algae *Gelidium* and composite material)

Biosorbent	pH_{SE} (mg l^{-1})	*S*/*L* (g l^{-1})	CR		C_S (mg l^{-1})	q_{M_0} (mmol g^{-1})
			Exp.	Calc.		
Gelidium	5.3	158	153.8	111.5	6360	0.192
	4.0	170	146.2	86.1	6369	0.155
	3.0	161	57.5	48.1	3000	0.083
Composite material	5.3	340[a]	53.9	52.6	2500	0.043
	4.0	254[a]	40.3	49.1	1750	0.037
	3.0	197[a]	11.6	9.3	500	0.013

[a] $\rho_{ap} = 0.25\ g\ cm^{-3}$.

Table 7
Mass transfer parameters for elution of lead (effect of pH)

Biosorbent	pH_{SE}	K_H^M	Q_{max} (mmol g^{-1})	ξ'_p	ε	P_e	k_f (cm s^{-1})	N_d	$\xi'_p N_d$	N_f
	5.3			216.3	0.893	35		4.9	1062.2	35.4
Gelidium	4.0	0.93	0.36	134.2	0.888	80	3.0×10^{-3}	4.9	655.5	37.2
	3.0			30.3	0.895	100		4.9	149.3	34.9
	5.3			98.6	0.816	80		11.4	1118.8	8.1
Composite material	4.0	1.1	0.16	64.7	0.839	55	4.0×10^{-4}	11.7	754.8	7.1
	3.0			16.1	0.859	50		12.0	192.4	6.2

of metal bounded. The maximum concentration values decrease with pH, as well as the concentration ratio (Table 6). As concluded above, the estimated values of CR are similar to those experimentally obtained for the composite material and lower for the algae *Gelidium* (Table 6).

After half of the residence time in the column, a slight decrease in pH occurred, due to the release of protons that remained bound to the active sites of the biomass. This instant corresponds to the beginning of the exit of metal ions with a concentration higher than the initial concentration of lead ions in the interstitial fluid as shown in Fig. 8(a) and (b). After that moment, the pH decreases abruptly. The acid front pushes the metal ions, originating high concentrations of metal ions. After pH stabilization to the value of the eluant, the desorption process is almost complete. Then, as

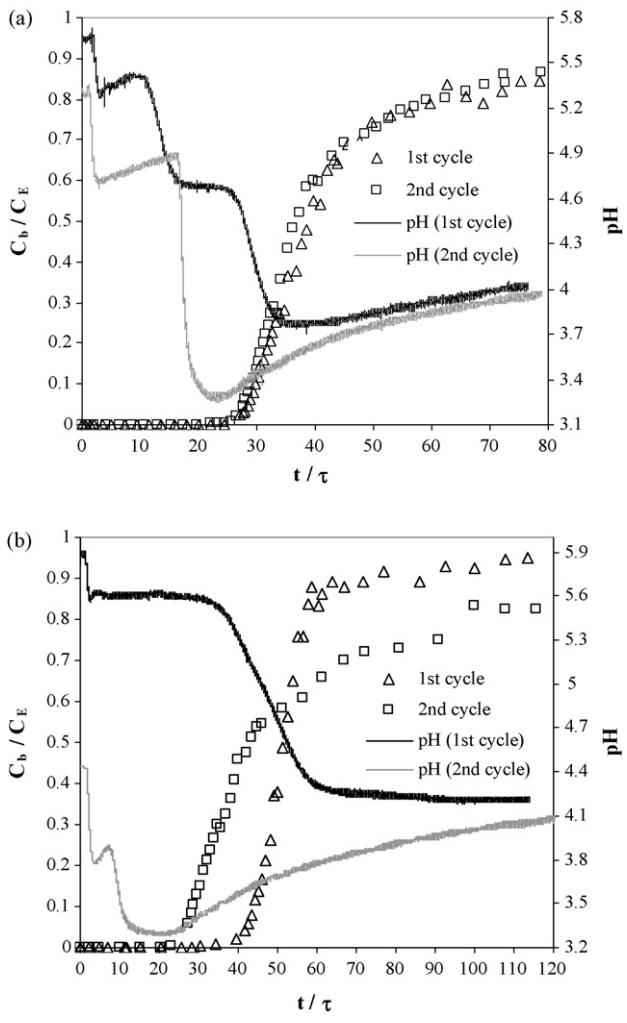

Fig. 9. Comparison of experimental lead breakthrough curves for two consecutive cycles and pH profile: (a) Experiments 13 and 15 and (b) Experiments 17 and 19.

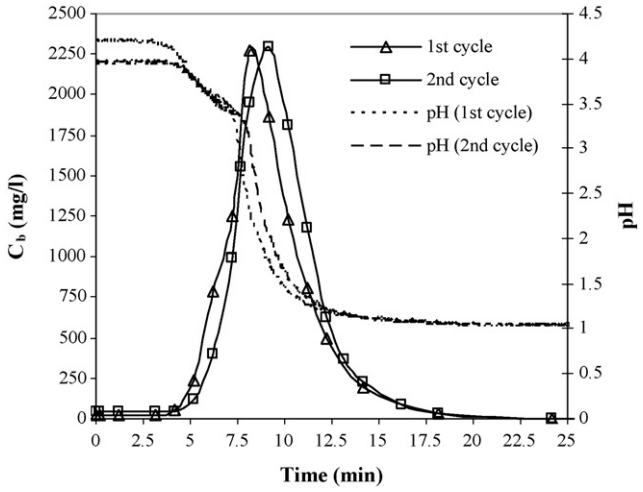

Fig. 10. Comparison of experimental elution curves for two consecutive cycles and pH profile (Experiments 14 and 16).

observed in the adsorption process, the pH breakthrough curve can be used as an indicator of the metal elution curve.

The model parameters used in the elution mass transfer model are presented in Table 7, but it is also necessary to know some operation parameters (Table 1), as the amount of lead-biomass loaded at the end of the saturation process (Table 6). The breakthrough curves are well predicted by the mass transfer model. The elution process is apparently controlled by lead ions diffusion in the film, since the ion exchange between the lead ions and protons is extremely fast.

4.3. Reutilization studies

The regenerated composite material was reused in two adsorption–desorption cycles and the results are show in Fig. 9(a) and (b) and Fig. 10. The efficiency of the adsorption–desorption process was the same for the two consecutive cycles, as illustrated in Figs. 9(a) and 10. The elution curves for the two cycles are very similar (Fig. 10), which means that the metal-loaded in the biomass is equal in the two consecutive cycles. This result indicates that the biomass did not suffer any damage in the cell structure, maintaining the same metal uptake.

The breakthrough time of the second cycle is lower than first cycle (Fig. 9(b)) as the initial pH of the second cycle (pH 4.4) is lower than the initial pH of the first cycle (pH 5.6), which leads to a decrease of the equilibrium uptake capacity of the biosorbent. After biomass regeneration, the column was rinsed with distilled water, but the pH at the column outlet did not reach the initial pH (5.6) of the adsorption step.

Fig. 9(a) shows that the uptake capacity in the two cycles remained constant, which means that protonation of the biomass did not affect the biosorbent capacity. However, ion exchange with protons increases the protons release, in contrast with the biomass

without acid treatment, where the toxic metal ions can exchange with other cations bound to the active sites.

5. Conclusions

Algal waste from agar extraction industry immobilized with polyacrylonitrile and algae *Gelidium*, the raw material for agar extraction, were used successfully for lead removal from aqueous solution in a packed bed column. The relationship between flow rate and breakthrough time can be used to find out the flow rate that maximizes the productivity and efficiency in a full-scale plant. Higher initial metal solution pH increases the uptake capacity of the biosorbents, leading to an increase in the breakthrough time and, consequently, to a higher efficiency of the water treatment process. The uptake capacity of the biosorbents remained constant after consecutive adsorption–desorption cycles, then allowing their reutilization. Two mass transfer models, considering film and intraparticle diffusion resistances and equilibrium given by Langmuir equation and mass action law, for adsorption and desorption, respectively, were successfully applied to describe the breakthrough curves, allowing a better understanding of the process and a reduction of the number of experiments necessary for process optimization.

Acknowledgements

Financial support for this work was in part provided by the Portuguese Foundation for Science and Technology (FCT) through the research project FCT/POCTI/AMB/57616/2004 and by LSRE financing by FEDER/POCI/2010, for which the authors are thankful. V. Vilar's acknowledges his Ph.D. scholarship by FCT (SFRH/BD/7054/2001).

References

[1] WHO, Environmental health criteria 165: inorganic lead, Geneva, 1995.
[2] WHO, Environmental health criteria 85: lead environmental aspects, Geneva, 1989.
[3] B. Volesky, Sorption and Biosorption, first ed., BV Sorbex, Inc., Quebec, 2003.
[4] Z. Aksu, F. Gonen, Z. Demircan, Biosorption of chromium(VI) ions by MOWITAL[r] B30H resin immobilized activated sludge in a packed bed: comparison with granular activated carbon, Proc. Biochem. 00 (2002) 1–12.
[5] J.W. Patterson, Industrial Wastewater Treatment Technology, second ed., Butterworth, Boston, 1985.
[6] J. Wase, C. Forster, Biosorbents for Metal Ions, Taylor & Francis, London, 1997.
[7] B. Volesky, Biosorption of Heavy Metals, CRC Press, Montreal, 1990.
[8] Z.R. Holan, B. Volesky, Biosorption of lead and nickel by biomass of marine algae, Biotechnol. Bioeng. (1994) 1001–1009.
[9] R. Jalali, H. Ghafourian, Y. Asef, S.J. Davarpanah, S. Sepehr, Removal and recovery of lead using nonliving biomass of marine algae, J. Hazard. Mater. 92 (3) (2002) 253–262.
[10] V.K. Gupta, M. Gupta, S. Sharma, Process development for the removal of lead and chromium from aqueous solutions using red mud—an aluminium industry waste, Water Res. 35 (5) (2001) 1125–1134.
[11] S.K. Srivastava, A.K. Singh, A. Sharma, Studies on the uptake of lead and zinc by lignin obtained from black liquor—a paper industry waste material, Environ. Technol. 15 (1994) 353–361.
[12] P.A. Marques, H.M. Pinheiro, J.A. Teixeira, M.F. Rosa, Removal efficiency of Cu^{2+}, Cd^{2+} and Pb^{2+} by waste brewery biomass: pH and cation association effects, Desalination 124 (1999) 137–144.
[13] S.K. Srivastava, V.K. Gupta, D. Mohan, Removal of lead and chromium by activated slag—a blast-furnace waste, J. Environ. Eng. 123 (5) (1997) 461–468.
[14] V.J.P. Vilar, C.M.S. Botelho, R.A.R. Boaventura, Influence of pH, ionic strength and temperature on lead biosorption by *Gelidium* and agar extraction algal waste, Proc. Biochem. 40 (10) (2005) 3267–3275.
[15] V.J.P. Vilar, C.M.S. Botelho, R.A.R. Boaventura, Kinetics and equilibrium modelling of lead uptake by algae *Gelidium* and algal waste from agar extraction industry, J. Hazard. Mater. 143 (1–2) (2007) 396–408.
[16] V.J.P. Vilar, F. Sebesta, C.M.S. Botelho, R.A.R. Boaventura, Equilibrium and kinetic modelling of Pb^{2+} biosorption by granulated agar extraction algal waste, Proc. Biochem. 40 (10) (2005) 3276–3284.
[17] V.J.P. Vilar, C.M.S. Botelho, R.A.R. Boaventura, Equilibrium and kinetic modelling of Cd(II) biosorption by algae *Gelidium* and agar extraction algal waste, Water Res. 40 (2) (2006) 291–302.
[18] V.J.P. Vilar, C.M.S. Botelho, R.A.R. Boaventura, Methylene blue adsorption by algal biomass based materials: biosorbents characterization and process behaviour, J. Hazard. Mater. 127 (1–2) (2007) 120–132.
[19] V.J.P. Vilar, Uptake of metal ions in aqueous solution by algal waste from agar extraction industry, Ph.D. thesis, Faculty of Engineering University of Porto, Porto, 2006.
[20] V.J.P. Vilar, C.M.S. Botelho, R.A.R. Boaventura, Biosorption of copper by marine red algae *Gelidium* and composite material in a packed bed column, Bioresour. Technol. (2007), doi:10.1016/j.biortech.2007.10.007.
[21] N. Madsen, R. Sincovec, PDECOL: general collocation software for partial differential equations, ACM Trans. Math. Soft. 5 (3) (1979) 326–351.
[22] V.J.P. Vilar, C.M.S. Botelho, R.A.R. Boaventura, Copper desorption from *Gelidium* algal biomass, Water Res. 41 (7) (2007) 1569–1579.
[23] A.E. Rodrigues, Elementos sobre a teoria de percolação, Luanda (1974).
[24] V.G. Teixeira, F.M.B. Coutinho, A.S. Gomes, Principais métodos de caracterização da porosidade de resinas à base de divinilbenzeno, Química Nova 24 (6) (2001) 808–818.
[25] G.F. Froment, K.B. Bischof, Chemical Reactor Analysis and Design, second ed., John Wiley & Sons, New York, 1990.
[26] R.C. Reid, J.M. Prausnitz, B.E. Poling, The Properties of Gases & Liquids, fourth ed., McGraw-Hill Book Company, New York, 1987.
[27] V.J.P. Vilar, C.M.S. Botelho, R.A.R. Boaventura, Copper removal by algae *Gelidium*, agar extraction algal waste and granulated algal waste: kinetics and equilibrium, Bioresour. Technol. 99 (4) (2008) 750–762.